JOURNAL OF PROPULSION AND POWER
Vol. 18, No. 2, March–April 2002

Chemiluminescence-Based Feedback Control of Equivalence Ratio for a Continuous Combustor

Douglas A. Scott*
Mobile, Alabama 36693
and
Galen B. King† and Normand M. Laurendeau‡
Purdue University, West Lafayette, Indiana 47907-1288

Recent pollution requirements and stringent operating conditions for gas-turbine engines have prompted the need for real-time feedback control of combustion processes for power production and propulsion. NO and CO pollutants from gas-turbine engines have been the focus of many researchers for some time. By accurate control of the equivalence ratio (EQR), fluctuations caused by low-frequency air flow rate disturbances may be avoided to maintain desired levels of NO and CO. In this paper, we develop a feedback technique based on CH chemiluminescence for real-time control of EQR in combustion processes. We focus on a continuous combustor for experimental modeling and implementation. An in-depth presentation is given of model development and digital controller design. Experimental step responses and an oxidizer flow rate disturbance test are provided for experimental validation of the EQR controller. The designed controller is successful in providing settling times less than 4.0 s with a maximum overshoot of 11.5%, while simultaneously compensating for oxidizer flow rate disturbances to within ~ 1%. With EQR control, a 153% increase in NO_x emissions is prevented in response to a 9% reduction in oxidizer flow rate at a global equivalence ratio near 0.75.

Introduction

RECENT pollution requirements and stringent operating conditions for gas-turbine engines have prompted the need for real-time feedback control of combustion processes for power production and propulsion. In general, NO and CO emissions constitute the main focus of environmental regulations for gas-turbine engines. Unfortunately, current sensing techniques do not allow for direct high-speed detection of NO and CO pollutants. However, it has been observed that NO and CO pollutants are very strong functions of overall equivalence ratio.[1,2] Developments in chemiluminescence sensing technology have provided an avenue for high-speed equivalence ratio (EQR) detection in combustion systems. This paper focuses on the development and implementation of a digital feedback system to control EQR in a simulated continuous combustor using CH chemiluminescence feedback. The current work advances that of Scott et al.[3] to handle air flow rate disturbances in a continuous flow combustor. By the accurate control of EQR, fluctuations caused by air flow rate disturbances may be avoided to maintain desired pollutant levels.

Chemiluminescence is the light produced during an electronic transition from a molecule's excited level to its equilibrium ground level. This transition is generally initiated through the chemical production of excited species. Ultimately, chemiluminescence signals obtained from optical measuring devices are proportional to the concentrations of the excited species. Typical chemiluminescence signals found in combustion originate from CH^*, OH^*, C_2^*, and CO_2^* (Refs. 4 and 5). In previous work in our laboratory, Scott et al.[3] found a linear relationship between CH chemiluminescence and EQR for global EQRs of $0.50 \leq \Phi \leq 0.85$ at constant oxidizer flow rates. Yamazaki et al.[6] investigated EQR relationships to OH, CH, C_2, and CO_2 emission spectra in jet flames and commercial diffusion-type burners. Their experiments revealed a linear relationship between both OH and CH emission signals and EQR for practical burners at global EQRs of $0.7 \leq \Phi \leq 1.4$. More importantly, Yamazaki et al.[6] found a dependency on the air flow rate for their tested global EQR. Their work revealed that as the total air flow rate varies, the proportionality changes between CH^* or OH^* and EQR. Sandrowitz et al.[7] also observed a linear relationship between CH^* and EQR as well as between OH^* and EQR. However, their experiments only incorporated premixed flames at $\Phi > 0.8$. In addition, Sandrowitz et al.[7] found that OH^* to CH^* ratios could be implemented to compensate for air flow rate dependencies. Although this ratio technique has merit, the current control methodology relies instead on CH chemiluminescence and fuel flow rate measurements. Extensive work was done to incorporate OH^* measurements within the digital control technique presented in this paper. Unfortunately, the OH^* and CH^* relations presented by Yamazaki et al.[6] and Sandrowitz et al.[7] were found to be inapplicable to our burner configuration for $0.50 \leq \Phi \leq 0.85$. Recently, Bandaru et al.[8] developed an EQR measuring device for gas-turbine combustors using CH and CO_2 chemiluminescence. Their work revealed that fuel and air flow rates strongly affect chemiluminescence intensities, whereas fuel/air mixedness is less important. Ultimately, fuel mass flow rate and emission voltages were used as an EQR indicator.[8]

There have been very few instances of feedback control for combustion systems in general, much less those that pertain to EQR or pollutant control. Previous studies include minimizing NO production[9,10] and optimizing NO emissions and combustion temperature.[11] These investigations incorporated gas analyzers and produced somewhat sluggish control; hence, effective disturbance compensation would be unlikely. Scott et al.[3] developed an EQR control technique that utilized CH chemiluminescence as feedback for constant oxidizer flow rate applications. Their work produced an EQR controller with a 1-s settling time, including compensation for fuel-line pressure disturbances. Under these circumstances, pollutant variations owing to fuel-line pressure disturbances may be minimized by controlling fluctuations in EQR. Unlike this previous work,

Received 9 June 2000; revision received 17 October 2001; accepted for publication 21 October 2001.

*2507 Muir Woods Court South.
†Associate Professor, School of Mechanical Engineering; kinggb@ecn.purdue.edu.
‡Ralph and Bettye Bailey Professor of Combustion, School of Mechanical Engineering.

our current work compensates for oxidizer flow rate fluctuations during EQR control periods. For a constant oxidizer flow rate, the CH signal increases linearly with rising EQR. However, as oxidizer flow rate is increased at the same EQR, the flame becomes more intense and a higher CH emission signal is observed. Without considering oxidizer flow rate, the perceived EQR would be greater than that in actuality. Moreover, oxidizer flow rate disturbances are much more difficult to handle because the relationship between EQR and CH emission is no longer linear.

Feedback control has numerous advantages over traditional open-loop control. Typically, gas-turbine combustors are maintained through open-loop control in which known proportions of fuel and air are dumped into the combustor at a chosen global EQR. Under most circumstances this type of operation is acceptable. However, even under set operating conditions, air fluctuations or additional unknown disturbances may occur. By feedback of a high-speed representation of EQR and compensating accordingly, these types of disturbances can be avoided. Because fluctuations caused by disturbances are minimized, feedback control allows for operation closer to an EQR producing minimum pollution levels than previously possible under open-loop conditions.

The objectives for EQR control in this paper have been developed from an intuitive viewpoint. Depending on the application and individual constraints, the control objectives and/or obtainable bandwidths may vary. For this work, the EQR controller was designed to meet the following two constraints:

1) The controller should settle to EQR commands in less than 5 s with little overshoot for all combinations of fuel and air flow rates ($0.65 \leq \Phi \leq 0.85$).

2) The controller should compensate for low-frequency disturbances, for example, air flow rate fluctuations.

A complete discussion of the modeling and controller design is covered in detail throughout the remainder of the paper. The criteria just listed play an important role in both the evaluation and design of the controller.

Experimental Setup

An atmospheric Hencken burner was selected to mimic typical gas-turbine combustors operating under partially premixed conditions. The Hencken burner is 2.54-cm square and composed of individual tubes (0.8 mm diameter) carrying either methane fuel or an oxygen/nitrogen mixture. Each fuel tube is surrounded by several oxidizer tubes that produce many tiny diffusion flames along the burner's surface. Unlike typical jet diffusion flames, this burner configuration allows for rapid mixing and manipulation of the global EQR. Because the burner is not fully premixed in nature, it has the ability to produce stable flames at very lean global operating conditions ($\Phi < 0.6$). Continuous burners, such as those found in industrial turbine applications, typically display such lean-operating characteristics. In typical gas-turbine operation, preheated air (600–700 K) is used for combustion of methane. In this experiment, a room-temperature mixture consisting of 2.72 moles of nitrogen for every mole of oxygen was used instead of air. Because higher quantities of oxygen are present, this 2.72 dilution ratio provides higher adiabatic flame temperatures. These elevated adiabatic flame temperatures roughly approximate those found in methane combustion when the air is preheated to 650 K.

For gas-turbine combustors, CO and NO pollutants rise as the overall EQR becomes either too lean or too rich, respectively.[1] As the EQR increases, the higher temperature causes greater quantities of NO to be formed. Conversely, as the EQR decreases, CO becomes more prevalent. Figure 1 illustrates the NO and CO emissions produced by the Hencken burner as a function of EQR at an N_2/O_2 dilution ratio of 2.72. These data were taken using typical low bandwidth NO and CO analyzers.[3] Both curves are normalized by their respective maximum emission indices.[12] Inspection of this plot reveals that pollutant trends for the Hencken burner closely match those found for traditional gas-turbine combustors.[1]

Figure 2 portrays the experimental setup used for control of the EQR. The experimental system consists of a Hencken burner, lens, chopper, filter, photodiode, lock-in amplifier, a set of digital microcontrollers, a data acquisition system, and a pulse-width-modulated (PWM) fuel-flow control valve.

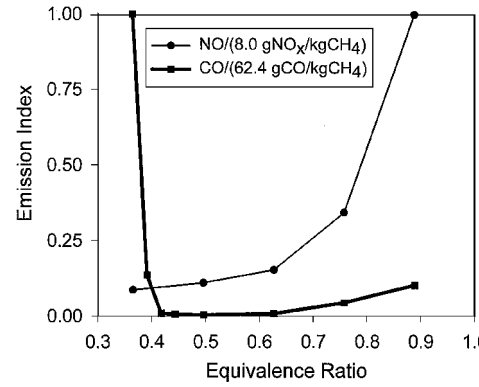

Fig. 1 Pollution emissions vs EQR for Hencken burner at N_2/O_2 = 2.72 v/v (Ref. 3).

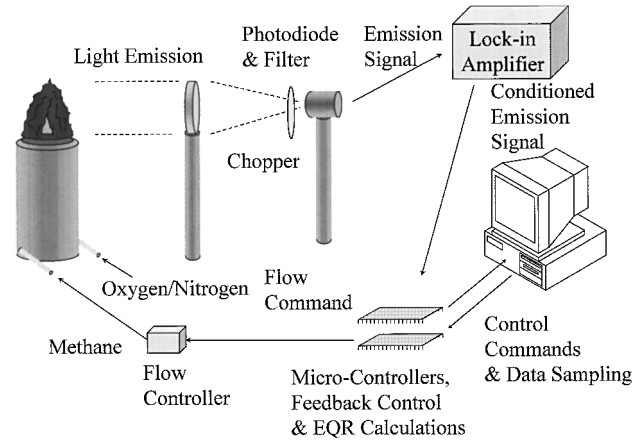

Fig. 2 Experimental setup for controller experiments.

Radiation from the flame is collected at the base of the burner with a fused-quartz lens and focused into a 431.5 ± 5 nm filter (Oriel Instruments, Model 53815) and a photodiode detector (Thorlabs, Model DET210). This filter–detector combination provides a voltage signal proportional to the CH emission from the flame. A chopper is used in conjunction with the lock-in amplifier to modulate and amplify the light signal. The chopper breaks the light signal at a prespecified frequency (397 Hz). The lock-in amplifier is then used to reconstruct and amplify signals at the chopped frequency. This modulation and amplification process provides excellent signal-to-noise characteristics because the light signal is modulated at a frequency different from those of typical 60-Hz noise or other environmental interferences.

The conditioned CH^* signal is fed into a Microchip Technology Inc. Model PIC16C73A microcontroller where it is digitally sampled, processed, and converted to a representation of EQR (at a 50-Hz loop rate). Figure 3 illustrates the microcontroller setup. For hardware reasons, two independent microcontrollers are necessary. The first microcontroller (PIC 1) samples the CH emission signal and records the fuel control command to develop a representation of EQR. The recorded fuel flow rate command is used to calculate EQR for the next time step ($\frac{1}{50}$ s). All of the control calculations and EQR conversions are performed on PIC 1. A 50-Hz sampling rate was selected to allow enough time for PIC 1 to perform all of the necessary control calculations and EQR conversions. The second microcontroller (PIC 2) receives a fuel command from PIC 1 through an 8-bit digital line where it is converted to a PWM fuel command for fuel flow rate control. PIC 2 operates at a 200-Hz loop rate. By sampling at a rate four times faster than PIC 1, the dynamics of PIC 2 are less significant to the overall control strategy.

The flow command controls the fuel flow through a PWM flow control valve (The Lee Company, Model LDHA122311H). A square

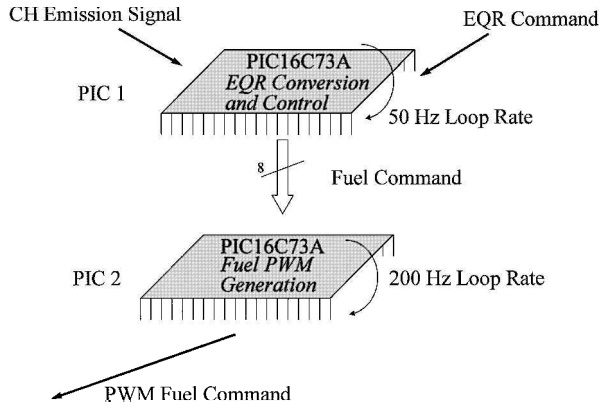

Fig. 3 Schematic of microcontroller configuration.

pulse modulated at a frequency of 100 Hz controls the fuel flow rate. The width of the pulse sent to the valve dictates the duration that the valve is open or closed. The valve only operates completely open or completely closed. A wider pulse sent to the valve keeps the valve open longer; likewise, a shorter pulse causes the valve to be closed more than it is open. Because the fuel flow cannot respond at 100 Hz, it is averaged according to the commanded pulse width. A 100-Hz PWM frequency provides the most accurate fuel control with the current experimental setup. In general, the valve provides fuel-flow control with near infinite resolution throughout the operating range and with very little valve hysteresis. The PWM valve essentially produces fuel flow proportional to a voltage input. Although the fuel control valve operates via a PWM signal, for convenience it is easier to work with a voltage signal proportional to the PWM duty cycle. All calculations and equations included in the remainder of this paper use this voltage representation of fuel flow rate command. A fluidic damper is added in series with the valve to act as a low-pass filter for additional stability (which may not be needed for higher bandwidth control).

CH Emission Signal and EQR

Previous experiments using the same burner at constant oxidizer flow rates revealed that a linear relationship exists between EQR and CH emission.[3] The objective here is to develop an EQR controller that accounts for variations in the total oxidizer flow rate. In particular, by incorporating the fuel flow rate command in addition to the CH emission signal, oxidizer flow rate variations can be handled quite efficiently. Figure 4 illustrates the calibration data used for EQR determination based on the CH emission signal for varying oxidizer and fuel flow rates. Three independent measurements were taken for each setting of fuel and oxidizer flow rate. The oxidizer flow rate is based on a 2.72 dilution ratio (v/v) of N_2 to O_2. Given a particular CH emission signal, an equivalence ratio can be extrapolated based on knowledge of the fuel flow rate. Figure 5 portrays the relationship of the slope and the Y intercept of the straight-line fits in Fig. 4 to the fuel flow rate command. The combination of Figs. 4 and 5 provides a two-dimensional mapping of CH emission and fuel flow rate to EQR. The final expression for EQR calculation then becomes

$$\Phi = 3.74 + 1.73\kappa - 1.98\kappa\varphi + 0.611\kappa\varphi^2 - 9.52\varphi + 7.89\varphi^2 - 2.05\varphi^3 \quad (1)$$

where Φ is the EQR, κ is the CH emission signal (volts), and φ is the fuel flow command to the fuel valve (volts). By manipulating Eq. (1) to generate a plot of emission voltage vs fuel flow rate for lines of constant EQR, we find trends nearly identical to those reported by Bandaru et al.[8]

Table 1 gives the maximum, average, and standard deviation (68% confidence limit) for the error between the actual EQR calculated from the fuel and oxidizer proportions and the EQR calculated from Eq. (1). Only data points used in the calibration of Fig. 4 are included in this analysis. Additional validation for interpolated points is considered later in this paper. In general, the data in Table 1 show that the EQR calculations are quite accurate, especially given the ~3% standard error for the EQR measurements (95% confidence limit).

Table 1 EQR calculation statistics ($\Phi_{actual} - \Phi_{calculated}$) for $0.65 \le$ EQR ≤ 0.85

Calculation	Value
Maximum	3.35×10^{-2}
Average	1.09×10^{-4}
Standard Deviation	1.49×10^{-2}

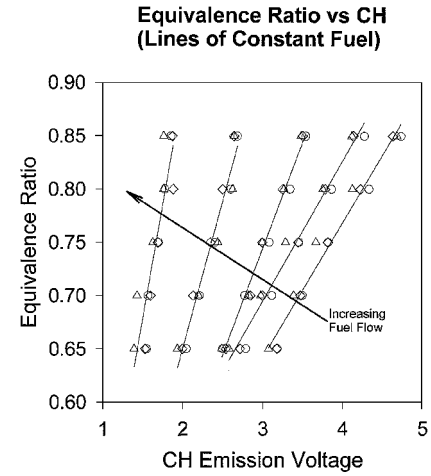

Fig. 4 Equivalence ratio vs CH emission voltage at various constant fuel flow rates. The points on a given line represent the influence of total oxidizer flow rate. Total oxidizer flowrates vary from 7.23 to 17.6 SLPM (based on a 2.72 N_2/O_2 dilution ratio). Methane fuel flow rates vary from 0.877 to 1.63 SLPM.

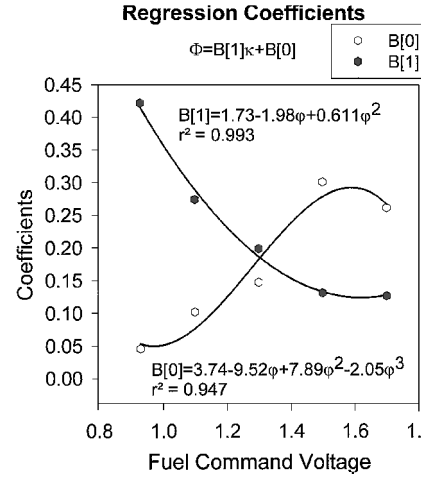

Fig. 5 Slope and Y intercept as a function of fuel flow rate. Φ is the equivalence ratio, κ is the CH emission signal (volts) and φ is the fuel-flow command to the fuel valve (volts).

Plant Modeling

To develop an adequate EQR controller, the dynamics of the combustion system must be evaluated. The term plant is often used to define the system that is to be controlled. For this system, the plant dynamics are the total lumped dynamics of the fuel control valve, burner, emission detection devices, and EQR scaling. To produce an accurate model, an input/output relationship was pursued. This representation was then transformed into a dynamic model for controller design.

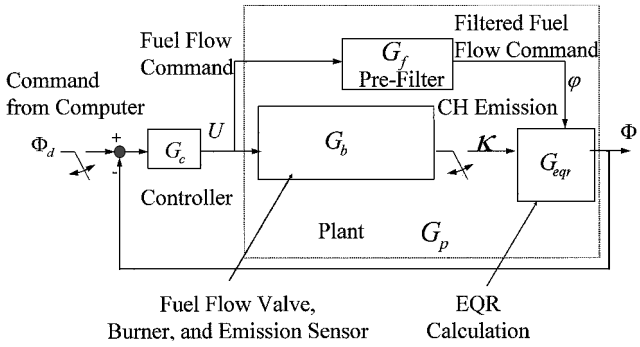

Fig. 6 Block diagram representation of EQR control system.

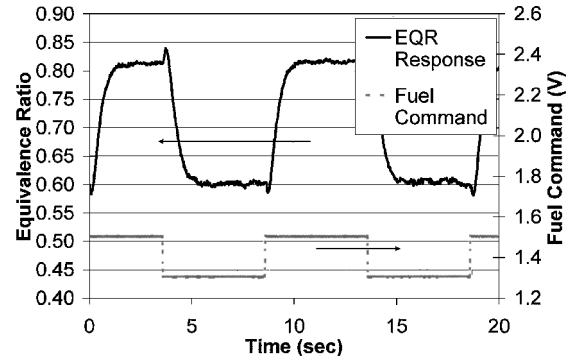

Fig. 7 Measured response to a square wave input to the fuel-flow valve; total oxidizer flow rate based on a 2.72 dilution ratio is 11.58 SLPM.

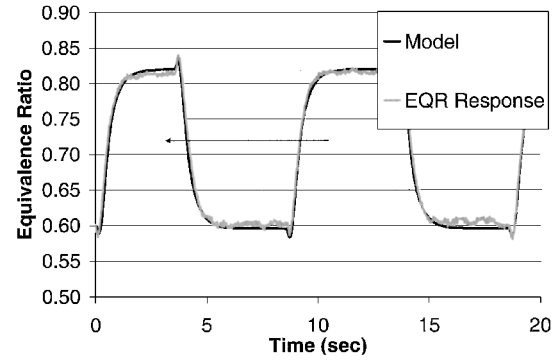

Fig. 8 Simulated and actual EQR response to a square wave fuel-flow input.

Figure 6 illustrates the block diagram of the EQR feedback control system. The plant dynamics G_p are developed from the input/output modeling procedure described hereafter. The controller dynamics G_c are then added within the microcontroller to give adequate performance in terms of the overall emission signal. The EQR-emission signal scaling G_{eqr} has its own dynamics, which depend on the dynamics of the fuel and CH emission interactions. G_f is a prefilter used for coordination of the fuel-flow command and CH emission signal during dynamic situations. For ease of discussion, the lumped dynamics of the fuel-flow valve, burner, and emission sensor are labeled as G_b. A plant model for the entire EQR control system includes the lumped dynamics of the fuel-flow valve, burner, emission sensor, prefilter, and EQR calculation.

Before the plant model can be developed, a prefilter design (G_f) is necessary. During control situations, a command to the fuel-flow valve affects the CH emission signal. Because the EQR calibration in Figs. 4 and 5 was developed for steady-state measurements, the dynamic lag from the burner transfer function G_b will produce an incorrect EQR during dynamic periods. Preliminary analysis without a prefilter indicated that a step command to the fuel-flow valve produced a large undershoot in EQR at the onset of the fuel command. However, after G_b had reached steady state, the EQR settled to its correct value. Therefore, a prefilter was devised such that the rise time of the fuel command used for EQR calculations roughly matched that of the CH* signal. The prefilter selected was a first-order unity-gain filter, whose dynamics follow:

$$G_f(s) = 1/(\tau s + 1) \tag{2}$$

The time constant τ was selected to minimize the undershoot following a step command. The time constant was selected to be 1.60 s. For implementation, the prefilter was converted to the Z domain using Tustin's approximation (see Ref. 13), and programmed into the microcontroller via a suitable difference equation. The difference equation was determined from the inverse Z transform[14] given by

$$\varphi_{[n]} = \frac{T}{(2\tau + T)}U_{[n]} + \frac{T}{(2\tau + T)}U_{[n-1]} - \frac{T - 2\tau}{(2\tau + T)}\varphi_{[n-1]} \tag{3}$$

where T is the sampling time, U is the unfiltered fuel flow command, and φ is the filtered fuel-flow command. The subscripts $[n]$ and $[n-1]$ indicate variable values at the current and previous time steps, respectively.

The dynamics of the combustion process and EQR scaling are too complex to model from first principles. Consequently, an experimental approach was incorporated to develop the plant model directly. In particular, a square wave input to the fuel control valve was imposed, followed by sampling of the EQR from the microcontroller. This procedure provides a dynamic input/output representation of the plant. Figure 7 shows the input to the fuel-flow valve and the response of the EQR signal from the microcontroller. The oxidizer flow rate was held at a constant value of 11.58 standard liters per minute (SLPM) throughout the duration of the square wave fuel input. This value of oxidizer flow rate is roughly in the middle of the calibration data employed in Fig. 4. The dynamics are slightly different with varying oxidizer flow rates, indicating that the model is actually nonlinear throughout the experimental range of oxidizer and fuel flow rates for $0.65 \leq \Phi \leq 0.85$. The effect of this nonlinearity will be seen later when considering the analysis of the experimental step responses.

Figure 7 indicates that an undershoot at the onset of a command change is noticeable even with the addition of a prefilter. A system with this type of response is sometimes characterized as nonminimum phase, that is, it has an unstable zero. The nonminimum phase response is a direct result of the EQR calculation rather than a real occurrence in G_b. Fortunately, this characteristic evident in the response can be handled in the controller design. Note that without the prefilter, the undershoot increases dramatically, and a controller with a reasonable bandwidth would be impossible to design.

Employing the input/output dynamic data given in Fig. 7, a dynamic model was developed as follows. The MATLAB® system identification toolbox was used to iteratively develop a model that displayed the appropriate dynamic behavior.[15] This toolbox is a very powerful software analysis package that can generate a dynamic model given real input/output data. The output-error method within MATLAB was selected to generate this model. Three poles, two zeros, and a time delay provided the best convergence for this dynamic system. A third-order system seems reasonable because the combustion process and PWM flow control valve may be modeled as first- and second-order systems, respectively. Once a fuel command is initiated, a set amount of time is required for the fuel to reach the burner. This time lag is captured as a pure time delay in the model. Figure 8 illustrates the actual and simulated output for the square wave input given in Fig. 7. The model and actual data closely follow one another for the given square wave input. The nonminimum phase effect is also captured by the model.

The data used to develop the dynamic model was sampled at 50 Hz. Therefore, the model developed in MATLAB is discrete in nature with a sampling rate of 50 Hz. Because the system is discontinuous and includes a time delay, it is easier to work in the Z domain. The z operator is defined as[13]

$$z = e^{sT} \tag{4}$$

where s is the Laplace operator and T is the sampling time. From Eq. (4), we see that information involving the Laplace operator and the sampling time are included in the z operator. The Z domain for discrete-time systems is directly analogous to the Laplace domain for continuous-time systems. The discrete plant model simulated in Fig. 8 with a sampling frequency of 50 Hz is given by

$$G_p = \frac{-0.07568z^2 + 0.09001z}{z^3 - 2.710z^2 + 2.458z - 0.7470} \tag{5}$$

Equation (5) gives the plant model used in the controller design. This model is taken as constant for all oxidizer flow rates that may occur, that is, we assume that the model parameters are invariant.

Controller Design

The controller design used for EQR control was developed in the Z domain because of the discrete nature of the plant model and microcontroller. Moreover, the time delay present in the model can easily be handled in the Z domain. The controller itself was designed using the classical root locus technique.[13,16] With this approach, the poles of the characteristic equation with feedback (closed-loop poles) can be studied as a function of control gain by observing the poles and zeros of the characteristic equation without feedback (open-loop poles and zeros). The controller consists of poles, zeros, and a control gain, each of which can be varied to give the best closed-loop performance. The root locus technique allows the designer to forecast the closed-loop pole locations as a function of gain when the controller's poles and zeros are added in the loop. The locations of the closed-loop poles within the unit circle dictate the dynamic behavior of the final closed-loop system. In the Z domain, closed-loop poles close to the imaginary axis are indicative of a faster responding system. Closed-loop poles close to the real axis provide a feedback control system with lower oscillations, that is, a higher damping ratio. This controller design methodology relies heavily on experience and human decision. For this reason, the controller solution is not unique. For our controller design, a free integrator (a pole at $Z = 1.0$) was implemented to provide zero steady-state error and low-frequency disturbance compensation. Additional poles and zeros were then added to provide closed-loop poles as close as possible to the imaginary and real axes for a set controller gain.

Figure 9 shows a root locus plot of the plant/controller combination. The addition of the free integrator at $Z = 1.0$ requires further complication of the controller. In particular, two additional zeros at 0.92 and one pole at -0.1 were added to the controller to provide good settling time and overshoot specifications. For clarity, the zeros are displayed with some separation; in reality, they overlap one another. The complete controller is given by

$$G_c = K\frac{(z - 0.92)(z - 0.92)}{(z - 1)(z + 0.1)} \tag{6}$$

where K is the control gain. The control gain K for this system was selected to be 0.4. This control gain places the closed-loop poles within Z-domain regions that provide low overshoot and settling time characteristics. As the control gain is increased to infinity, the system becomes unstable. However, this instability point is far from the design gain of 0.4. Further emphasizing the stability of the controller, the design provides for a phase margin of 75 deg and a gain margin of 13.6 dB. The crossover frequency for this system is 1.30 rad/s. The controller should be able to handle airflow disturbances at rates on the order of five times less than this crossover frequency ($\sim 10^{-3}$ Hz).

For gains close to the specified control gain of 0.4, the free integrator and plant pole close to 1.0 dominate the response. To give an indication of the scaling, the control zeros at 0.92 in the Z domain with a sampling rate of 50 Hz translate to approximately 4 rad/s in the Laplace domain. Because the dominant poles track into the control zeros, little gain is needed to produce settling times less than 5 s. In addition, the dominant poles are close to the real axis. Hence, we should expect that the system will be relatively well damped.

The final closed-loop poles in the Z domain are given in Table 2. For intuitive understanding, Table 2 also lists their continuous time-domain counterparts. From this information, the damping ratio of the closed-loop poles can be determined, as also given in Table 2.

With the controller designed, the feedback loop can be closed and simulations can be undertaken of the closed-loop system. A simulated EQR step response is illustrated in Fig. 10. In this case, the simulation represents the response arising from an EQR command from 0.65 to 0.75. The 2% settling time of 2.10 s based on the step change $\Delta\Phi = 0.1$ is highlighted to illustrate conformance with the established design criteria. However, validation of the disturbance rejection capabilities of the controller requires real system data, as demonstrated in the next section.

For implementation of the digital controller, the microcontroller was programmed with a difference equation that was derived from Eq. (6). The difference equation was developed using the same

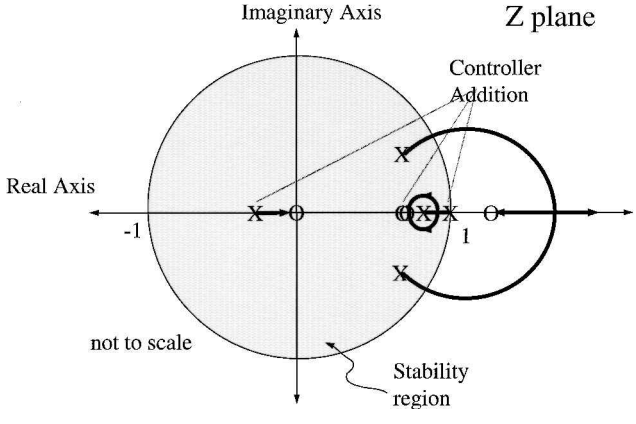

Fig. 9 Root locus of open-loop system with compensation; poles track into the zeros as a function of gain. The free integrator (at $Z = 1.0$) meets one of the plant poles and they both travel into the two controller zeros; the other controller pole travels into a plant zero at the origin. Two underdamped plant poles move beyond the unit disk and meet in the unstable region; one travels into the unstable zero, and the other traverses outward along the real axis.

Table 2 Digital/continuous closed-loop poles ($K = 0.4$)

Z-domain poles	Laplace-domain poles	Damping ratio
-0.0965	$-116.9 + 157.1i$	0.59
$0.9668 + 0.01515i$	$-1.684 + 0.7834i$	0.91
$0.9668 - 0.01515i$	$-1.684 - 0.7834i$	0.91
$0.9015 + 0.1240i$	$-4.717 + 6.833i$	0.57
$0.9015 - 0.1240i$	$-4.717 - 6.833i$	0.57

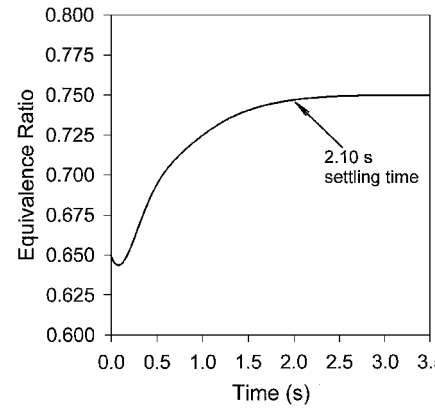

Fig. 10 Simulated EQR control system for a step change from $\Phi = 0.65$ to $\Phi = 0.75$.

techniques as discussed in the prefilter design. Equation (7) gives the difference equation used for controller implementation, that is,

$$U_{[n]} = -U_{[n-1]}(\rho_1 + \rho_2) - U_{[n-2]}\rho_1\rho_2 + K\left[e_{[n]} + e_{[n-1]}(\zeta_1 + \zeta_2) + e_{[n-2]}\zeta_1\zeta_2\right] \quad (7)$$

where U is the fuel command to the flow control valve from the microcontroller, e is the error between the desired EQR and the calculated EQR, ρ_1 and ρ_2 are the controller poles, ζ_1 and ζ_2 are the controller zeros, and K is the controller gain. The subscripts $[n]$, $[n-1]$, and $[n-2]$ indicate variable values at the current and preceding two time steps.

Experimental Results for Controller Testing and Verification

Figure 11 illustrates the experimental step responses arising from an EQR command from 0.65 to 0.75 and from 0.65 to 0.85 for total oxidizer flow rates of 13.4 and 15.3 SLPM, respectively. The data displayed represent the average of three step responses sampled at 50 Hz with the data acquisition system. Initially, the desired EQR was set at 0.65. At approximately 0.78 s, the EQR command was changed to either 0.75 or 0.85. The two plots exhibit slightly different responses. For the lower oxidizer flow rate (EQR from 0.65 to 0.75), the behavior is exceptionally close to the model response given in Fig. 10. In fact, the response displays very little overshoot with a settling time of 1.84 s. However, for the higher oxidizer flow rate (EQR from 0.65 to 0.85), a larger 11.5% overshoot is experienced, and the system settles in 3.42 s. Both step responses possess the nonminimum phase effect, that is, undershoot at the onset of the command change. However, these nonminimum phase effects seem to be smaller than those observed in the simulation (see Fig. 10).

The two experimental step responses displayed in Fig. 11 are representative of the range of step responses observed for other test cases. The best observed responses were for low oxidizer flow rates such as those displayed in Fig. 11 for an oxidizer flow rate of 13.4 SLPM. The worst step responses observed were for conditions similar to the 15.3 SLPM case in Fig. 11. These differences in response can be attributed to the EQR calculation being nonlinear. Hence, as expected, the best step responses occurred for oxidizer flow rates close to those used in the model development. For such cases, the experimental responses were similar to the simulated step response in Fig. 10.

The data presented in Fig. 11 correspond to EQR values calculated using Eq. (1). Measured fuel and oxidizer flow rates provide actual EQR data. EQR calculations for the 13.4 SLPM case reveal that EQRs are actually 0.657 and 0.730 for EQRs displayed in Fig. 11 as 0.65 and 0.75, respectively. Similarly, for the 15.3 SLPM case, EQRs are actually 0.681 and 0.823 for EQRs displayed in Fig. 11 as 0.65 and 0.85, respectively. Because these EQR data points were not included in the original calibration in Figs. 1 and 2, the agreement suggests that the EQR calculation method presented earlier is, in fact, reasonably accurate for interpolated operating conditions, that is, for points not included in the original calibration in Fig. 4.

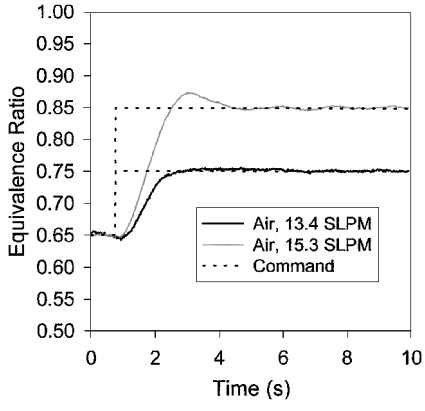

Fig. 11 Two experimental step responses for oxidizer flowrates of 13.4 and 15.3 SLPM; the total oxidizer flow rate is based on a 2.72 dilution ratio of N_2 to O_2.

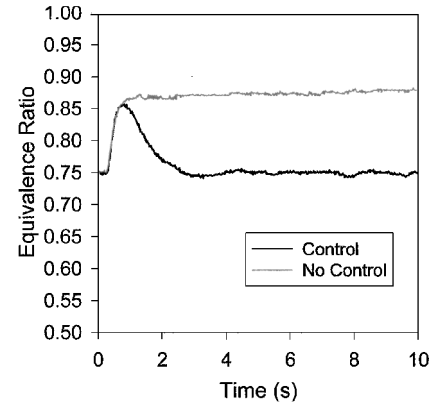

Fig. 12 Response to a 9% reduction in oxidizer flow rate with and without control (oxidizer is based on a 2.72 dilution ratio of N_2 to O_2).

Figure 12 illustrates the ability of the EQR controller to compensate for unknown disturbances and to maintain the EQR at 0.75 to within ~1% (95% confidence limit). Initially the total oxidizer flow rate is held at 15.3 SLPM. At approximately 0.3 s, the oxidizer flow rate is reduced to 13.9 SLPM, a 9% reduction. With the control system in operation, the disturbance increases the EQR to 0.85. In roughly 3.0 s, the disturbance is quenched by the controller and the EQR is brought back to 0.75. Without EQR control, however, the 9% reduction in oxidizer flow rate increases the EQR to 0.875. Hence, as expected, no compensation exists to reduce the EQR to the desired set point of 0.75.

As for the step responses, the data presented in Fig. 12 correspond to EQR values calculated using Eq. (1). During the oxidizer disturbance test without control, an EQR of 0.75 corresponds to an actual EQR of 0.751. An EQR of 0.875 in Fig. 12 corresponds, in actuality, to 0.856. During controller operation, actual EQRs before and after the oxidizer disturbance are 0.751 and 0.750, respectively. The controller accurately adjusts the fuel flow rate to handle a reduction in oxidizer flow rate. However, the reduction in oxidizer flow rate does not correspond to a calibrated point (in Fig. 4). The accurate fuel-flow adjustment is simply based on interpolation between actual calibration data.

Without EQR control, a 9% oxidizer flow rate reduction produces an NO_x emission index of 6.67 $gNO_x/kgCH_4$ (at actual $\Phi = 0.856$). When compared to the NO_x emission index at $\Phi = 0.751$ (2.64 $gNO_x/kgCH_4$), the uncontrolled system exhibits a 153% increase in NO_x emissions. With EQR control, NO_x emissions are held to 2.64 $gNO_x/kgCH_4$ (at $\Phi = 0.750$) after 3.0 s. Therefore, with control, a 153% increase in NO_x emissions is prevented in response to an oxidizer flow rate reduction of only 9%.

For extreme disturbances, the EQR controller could converge to an incorrect EQR. The EQR calculation in Eq. (1) is not single valued, that is the same EQR value may be obtained from two or more different fuel/CH* combinations. Improper convergence only occurred when the fuel and/or CH emission signal deviated from the range specified in the calibration (Fig. 4). In our experiments, such conditions only occurred when a loss of signal was imposed (by a momentary blockage of the photodiode). However, although the EQR value was incorrect, stability was always preserved. To prevent this problem, the allowed values for fuel and CH emission must be limited to their calibrated ranges.

Conclusions

A digital control system has been developed for the control of EQR using measurements of CH chemiluminescence. A unique EQR calculation method is presented to handle oxidizer flow rate variations given only the CH emission signal and the fuel flow rate command. The control system is validated through simulation and experimental tests. The designed controller is successful in providing settling times less than 4.0 s with a maximum overshoot of 11.5%

and in compensating for significant oxidizer flow rate disturbances. With EQR control, a 153% increase in NO_x emissions is prevented in response to a 9% reduction in oxidizer flow rate at an initial global EQR of 0.75.

The EQR calculation requires extensive calibration to account for variations in both oxidizer and fuel flow rate. This method produces accurate high-speed EQR calculations using only CH emission and fuel flow rate signals. However, the EQR calculation technique cannot handle fuel flow rate disturbances. It assumes that any command to the fuel-flow valve represents the actual fuel flow rate at the combustor. Compensation for fuel-line pressure disturbances would not be sensed as such with the proposed EQR calculation. Scott et al.[3] previously developed a method for EQR control in the presence of fuel-line pressure disturbances. However, the oxidizer flow rate disturbance compensation discussed in this work cannot be handled by our previous controller.[3] An additional input is required for EQR control in the presence of both fuel and oxidizer disturbances. Incorporating OH chemiluminescence in addition to CH chemiluminescence is not feasible for the current burner configuration because of the essentially linear relationship between the OH^* and CH^* signals. A better method could incorporate a slightly downstream measurement of CO_2^* in addition to an upstream CH^* measurement.[8] The incorporation of CO_2 chemiluminscence could provide independent information such that a CH/CO_2 chemiluminescence ratio would give an EQR measurement that accounts for any variations in oxidizer flow rate.

Because the objective for EQR control is usually to minimize pollutant production, a more effective control system can be achieved with direct optical measurements of NO and CO emissions. To date, no such sensors are commercially available for high-temperature, high-speed measurements of NO and CO.

References

[1]Lefebvre, A. H., "The Role of Fuel Preparation in Low-Emission Combustion," *Journal of Engineering for Gas Turbines and Power*, Vol. 117, 1995, pp. 617–654.

[2]Correa, S., "A Review of NO_x Formation Under Gas-Turbine Combustion Conditions," *Combustion Science and Technology*, Vol. 87, No. 1–6, 1992, pp. 329–362.

[3]Scott, D. A., King, G. B., and Laurendeau, N. M., "Digital Control of Equivalence Ratio Using Chemiluminescence Feedback for a Continuous Combustor," *Combustion Science and Technology*, Vol. 159, 2000, pp. 129–146.

[4]Roby, R. J., Hamer, A. J., Johnsson, E. L., Tilstra, S. A., and Burt, T. J., "Improved Method for Flame Detection in Combustion Turbines," *Journal of Engineering for Gas Turbines and Power*, Vol. 117, 1995, pp. 332–340.

[5]Gaydon, A. G., *The Spectroscopy of Flames*, Chapman and Hall, London, 1974.

[6]Yamazaki, M., Ohya, M., and Tsuchiya, K., "Detection of the Air Equivalence Ratio of a Burner from the Flame-Emission Spectra," *International Chemical Engineering*, Vol. 30, 1990, pp. 160–168.

[7]Sandrowitz, J. M., Cooke, J. M., and Glumac, N. G., "Flame Emission Spectroscopy for Equivalence Ratio Monitoring," *Applied Spectroscopy*, Vol. 52, 1998, pp. 658–662.

[8]Bandaru, R. V., Miller, S., Lee, J., and Santavicca, D. A., "Sensors for Measuring Primary Zone Equivalence Ratio in Gas Turbine Combustors," *Proceedings of SPIE*, Vol. 3535, 1998, pp. 104–114.

[9]Brouwer, J., Ault, B. A., Bobrow, J. E., and Samuelsen, G. S., "Active Control for Gas Turbine Combustors," *Proceedings of the Twenty-Third International Symposium on Combustion*, Combustion Inst., Pittsburgh, PA, 1990, pp. 1087–1092.

[10]St. John, D., and Samuelson, G. S., "Active, Optimal Control of a Model Industrial, Natural Gas-Fired Burner," *Proceedings of the Twenty-Fifth International Symposium on Combustion*, Combustion Inst., Pittsburg, PA, 1994, pp. 307–316.

[11]Jackson, M. D., and Agrawal, A. K., "Active Control of Combustion for Optimal Performance," *Journal of Engineering for Gas Turbines and Power*, Vol. 121, 1999, pp. 437–443.

[12]Turns, S. R., *An Introduction to Combustion, Concepts and Applications*, McGraw–Hill, New York, 1996, pp. 475, 476.

[13]Franklin, G. F., Powell, J. D., and Workman, M., *Digital Control of Dynamic Systems*, Addison Wesley Longman, Menlo Park, CA, 1998, p. 231.

[14]Oppenheim, A. V., and Schafer, R. W., *Discrete-Time Signal Processing*, Prentice–Hall, Englewood Cliffs, NJ, 1989, pp. 165–191.

[15]*MATLAB User's Guide*, MathWorks Inc., Natick, MA, 1990, p. 71.

[16]Nise, N. S., *Control Systems Engineering*, Benjamin/Cummings, Redwood City, CA, 1995, p. 380.